Mapping the Sun with Radio Interferometry

Avery Books
University of California, Berkeley, Dept. of Astronomy
April 9, 2026

ABSTRACT

This paper details the calibration and application of a two-element X-band (10.5 GHz) radio interferometer to measure the angular diameter of the Sun. By tracking the solar transit over a 12-hour period, we extracted the characteristic broadband interference fringes and utilized a non-linear least-squares optimization to precisely calibrate the instrumental baseline (b_{ew}, b_{ns}) and cable delays. Applying a 1-D uniform disk approximation and Fourier bandpass filtering to the visibility data, we isolated the fringe modulator to identify the spatial frequency of the first zero-crossing. We derived a solar angular diameter of 31 arcminutes, close to the accepted value of 32 arcminutes with a highly accurate 3.125% error. Remaining discrepancies are analyzed in the context of solar limb darkening and bandwidth smearing. These results successfully validate both the robust hardware calibration of the New Campbell Hall array and the foundational theoretical framework of aperture synthesis.

Contents

1. Introduction

This experiment aims to develop proficiency in radio interferometry, a foundational technique in modern radio astronomy famously used by the Event Horizon Telescope to image a black hole Interferometry provides high resolution imaging capabilities through arrays of telescopes instead of singular dishes. This allows us to effectively convert the standard equation for telescope angular resolution to one that considers the entire array

$$\lambda/D \approx \theta \Rightarrow \lambda/B_{max} \approx \theta \qquad (1)$$

Where θ is the angular resolution, D is the distance across a single dish telescope, and B_{max} is the length of the telescope array baseline. The baseline is the physical separation between dishes. For reference, the ALMA array utilizes 15-16 km baselines to achieve angular resolutions between 0.02" and 29"

This project explores the fundamental properties of the interferometric fringe as caused by the Sun and it's motion across the sky. We utilize dual robotic telescopes for data collection, Fourier transforms, Bessel functions, and Least-Square fitting for data analysis and value recovery. In particular, we recover the antenna baseline, sky brightness, and angular diameter of the Sun.

2. System Characteristics

2.1. System Hardware

The setup is an X-band interferometer (10.5 GHz center frequency) comprising two dishes on the roof of UC Berkeley's New Campbell Hall. The signal undergoes two stages of frequency down-conversion into the baseband range for digital sampling.

The first downconversion has an LO of 8.75 GHz that converts the signal to an intermediate frequency which then gets downconverted again with an LO of 1.54 GHz into the baseband frequency range. Then the signal gets processed by our SNAP board that implements an FX correlator (Fourier transform cross multiply). First the board digitizes two voltage signals, one from each dish via an ADC and computes Fourier transforms each with 1,024 frequency channels providing complex-valued voltage spectra. The spectra of one dish is multiplied with the complex conjugate of the voltage from the second spectra to get a visibility spectra. These spectra are averaged over 305,200 individual spectra which corresponds to an approximately 1.25 second integration. These averaged spectra are analyzed to get the fringe, baseline, and angular diameter information.[1]

2.2. Software Control and Data Acquisition

The system is controlled using the ugradio Python module and `snapspec` package.

Telescope control specifically uses the ugradio.interf submodule that contains the Interferometer() class and pointing, stow, and maintenance commands. Data collection is handled by the snap spec package where we initialized the system to take

---

[1] An in-depth diagram of the telescope system is available on Prof Aaron Parson's github under the "Lab interf" section. The diagram is credited to Prof Parsons.

cross-correlation data between the dishes and is combined with `ugradio.coord` for metadata including Julian Date, sun positions in RA and Dec, and the altitude and azimuth coordinates of telescope pointing.

To ensure a continuous observation system, threaded data collection scripts were critical. Unlike standard synchronous execution, Python's threading module enables dedicated background processes for data acquisition. This prevents telescope slewing or file writing operations from interrupting continuous data collection.

This is particularly important to ensure long data collection continuity in data and to avoid any gap induced artifacts that would significantly affect our Fourier transformed information. This keeps the phase slope across frequency channels consistent such that the least-square fitting is possible and accurate for baseline calculations.

3. Fringe Theory

To understand the data collected in this report, we must first characterize the interferometric "fringe." This phenomenon can be conceptualized through three distinct, yet mathematically equivalent, frameworks:

1. **A Geometric Spatial Filter:** The interferometer projects a "giant sine wave" onto the celestial sphere. As the Earth rotates, the source moves through the spatial peaks and nulls of this wave. The incoming radio waves alternate between constructive and destructive interference, causing the recorded signal to oscillate at what is known as the local fringe frequency.
2. **A Cross-Correlator:** Fundamentally, the fringe is the direct cross-correlation of the voltage signals received by the two antennas. The output of this correlation is proportional to the relative phase difference between the two signal paths.
3. **A Double Sideband (DSB) Mixer:** The rotation of the Earth provides a kinematic "local oscillator" effect. As the source traverses the sky, the continuously changing path-length difference "mixes" the high-frequency celestial signal, downconverting it into the much lower, observable fringe frequency.

While many celestial radio sources can be treated as infinitesimal "point sources," the Sun is an extended source. Its angular diameter is approximately 32 arcminutes according to the accepted literature, which is significantly larger than the resolution scale of our interferometer at the meridian, which is 7 arcminutes. To model the Sun's impact on our data, we simplify its two-dimensional brightness distribution into a one-dimensional model. Since our East-West baseline primarily resolves the sky along the direction of the source's motion (the hour angle), the interferometer is effectively "blind" to the Sun's structure in the North-South direction. We therefore integrate the Sun's 2D intensity along vertical strips to create a 1-D brightness distribution, $I(\Delta h)$.Assuming the Sun is a uniformly bright disk of angular radius R, the 1-D intensity profile is not a simple rectangle. Instead, because there is more "solar material" near the center of the disk than at the edges, the 1-D projection follows the geometry of a circle:

$$I(\Delta h) \propto \sqrt{R^2 - \Delta h^2} \quad \text{for} \quad |\Delta h| \leq R \tag{2}$$

where Δh is the angular offset from the Sun's center. This 1-D approximation serves as the theoretical basis for our source structure analysis, which has a Fourier transform of a first order Bessel function $(J_1(x)/x)$ that will allow us to calculate the Sun's R from the first null as further explained in 3.4.

3.1. Geometric Delay and Local Fringe Frequency

The unifying physical mechanism behind these frameworks is the geometric time delay (τ_g), the difference in arrival time of an incoming wavefront at the two antennas. As Earth rotates, this continuously varying path-length difference drives the correlator's phase shifts and produces the characteristic fringe oscillations.

Operating under the simplifying assumption of a purely East-West baseline (b_{ew}), the geometric delay can be calculated purely as a function of the source's hour angle (h_s) and declination (δ):

$$\tau_{g,ew}(h_s) = \left[\frac{b_{ew}}{c}\cos\delta\right]\sin h_s \tag{3}$$

where c is the speed of light. This geometric delay serves as the critical parameter for modeling the interferometer's actual response. Substituting τ_g into our signal equations allows us to express the complex visibility of the source, which is the mathematical representation of the fringe, expanded into its real and imaginary components:

$$F(h_s) = A\cos(2\pi\nu\tau_g) + B\sin(2\pi\nu\tau_g) \tag{4}$$

where ν is the observing frequency, and the coefficients A and B encapsulate the amplitude and phase structure of the source. Further, the continuous change in this geometric delay as the source drifts overhead is exactly what dictates the local fringe frequency mentioned previously. Taking the time derivative of the phase argument $(2\pi\nu\tau_g)$ yields this instantaneous frequency, directly linking the Earth's rotation to the oscillations observed in our data.

While the physical baseline (b_{ew}, b_{ns}) is measured in meters on the ground, the interferometer's ability to resolve source structure depends on the projected baseline as seen from the direction of the source. This projection is represented in the $u - v$ plane, where u and v are the East-West and North-South components of the baseline, respectively, measured in units of the observing wavelength (λ).The coordinates (u, v) correspond to spatial frequencies. As the Earth rotates, the projection of our fixed baseline onto the celestial sphere changes, causing (u, v) to trace an elliptical arc over time. For our nearly East-West interferometer, the u coordinate is the dominant factor in resolving the Sun and is related to the hour angle (h_s) and declination (δ) by:

$$u = \frac{b_{ew}}{\lambda}\cos\delta\cos h_s \tag{5}$$

The distance from the origin in this plane, $q = \sqrt{u^2 + v^2}$, defines the instantaneous resolution of the array. Specifically, the fringe spacing on the sky is given by $\theta_{fringe} \approx 1/q$ radians.This coordinate system is critical for our analysis of the Sun's diameter. The 1D approximation model (Equation 2) exists in the spatial domain, but the interferometer samples the source in the Fourier domain (the $u-v$ plane).

The continuous change in geometric delay and the projected u coordinate as the Earth rotates allows us to formally derive the local fringe frequency, f_f. Mathematically, this fringe rate is defined as the time derivative of the phase delay:

$$f_f = \frac{d}{dt}(\nu\tau_g) \tag{6}$$

In practical analysis, this theoretical frequency provides a crucial diagnostic tool. Taking the Fourier transform of our recorded visibility signal should yield a distinct power peak exactly at the frequency predicted by the geometric delay model, serving as a primary "sanity check" for tracking and baseline assumptions. While a singular geometric delay effectively models a point source, the analysis becomes significantly more complex when observing extended celestial bodies. For extended sources like the Sun, different spatial regions across the solar disk correspond to slightly different geometric delays. Due to the Sun's finite angular width, the interferometer effectively detects a continuous superposition of these varying delays simultaneously. To account for this spatial complexity, the total response of the interferometer is modeled as the product of the ideal point-source fringe, $F(h_s)$, and a Fringe Modulator, MF. The fringe modulator acts as a spatial filter that scales the amplitude of the fringes based on the intrinsic structure of the source. Mathematically, this modulator is the Fourier transform of the source's 1-D intensity distribution. For a radially symmetric source, such as the uniform solar disk in our 1D approximation, this simplifies to a cosine Fourier transform:

$$MF = \int I(\Delta h)\cos(2\pi f_f \Delta h) d\Delta h \tag{7}$$

Physically, the interference among the multitude of individual point-source fringes across the solar disk is what modulates the overall amplitude. In the complex visibilities that we record, this mathematically manifests as a distinct "beat pattern," where the rapidly oscillating, high-frequency fringe is bound by a slower-moving amplitude envelope defined by MF.

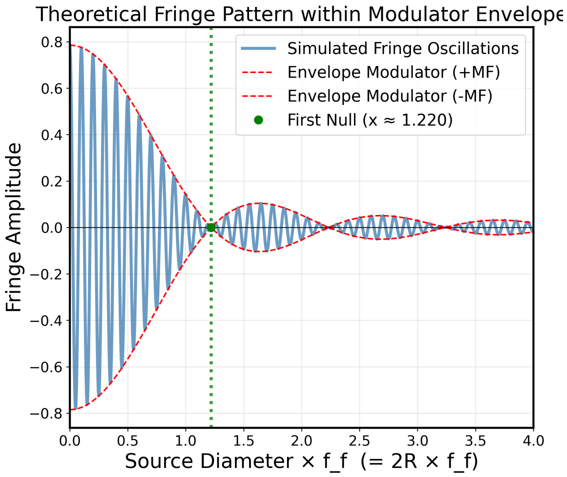

Fig. 1.— The blue simulated fringe oscillations inside the red envelope demonstrate the sun moving across the "giant sine wave" in the sky discussed earlier. The red envelope is the Bessel function that comes from the cosine Fourier transform. Since we can determine f_f we are able to back out the source diameter R from data of this form.

3.2. Total Delay and Instrumental Effects

While the geometric delay (τ_g) accounts for the path-length difference in the sky, it does not represent the entirety of the signal's journey. In a physical interferometer, the signals from each antenna must travel through cables, amplifiers, and filters before reaching the correlator. Because these cables are of unequal physical lengths and electronic components introduce internal phase shifts, we must account for an instrumental cable delay (τ_c). Further, our baseline is primarily East-West, so any slight North-South displacement (b_{ns}) or vertical offset (b_{up}) contributes additional terms to the delay. The true total delay (τ_{tot}) is the sum of these geometric and instrumental components:

$$\tau_{tot} = \tau_{g,ew} + \tau_{g,ns} + \tau_{g,up} + \tau_c \tag{8}$$

In the context of our experimental setup, we simplify this expression by grouping the relatively constant terms. Near the meridian, the North-South and vertical geometric delays vary much more slowly than the East-West component. Consequently, we define a modified delay (τ_g') that encapsulates the primary time-varying East-West delay alongside a composite offset term that accounts for cable lengths and baseline misalignments. In short, when we write the modified delay (τ_g') we are bundling the almost constant North-South geometric delay with the more variable East-West delay. During the least-squares fitting process 9, the cable delay is treated as a free parameter. In the initial linear stage, it is recovered from the phase relationship between the A and B coefficients; in the subsequent nonlinear stage, it is explicitly characterized to provide a precise measurement of the internal hardware delay.

While the geometric and instrumental delays describe a single frequency, our system utilizes a SNAP board that produces a broad spectrum of 1,024 frequency channels. Because the total delay (τ_{tot}) affects the entire broadband signal, the phase of the complex visibility (Φ) changes across these frequency channels. This creates a measurable "phase slope" across the band, defined mathematically as $\frac{d\Phi}{d\nu} = 2\pi\tau_{tot}$. By extracting this slope from our multi-channel visibility data, we can accurately measure the true time delay of the incoming signal before passing it into our baseline fitting algorithms.

3.3. Least Squares Fitting and Baseline

Least Squares fringe fitting

The baseline components that we want to measure via the fringe characteristics are recovered from inside trigonometric functions 4, so standard linear regression is not sufficient. We must implement a non-linear optimization via a least-squares fringe fitting. Where the modified delay of τ_g' contains the unknown baseline lengths b_{ns} and b_{ew} and the cable delay τ_c. To extract the precise baseline components, we must first minimze the sum of the squared residuals (S) between the observed data (V_{obs}) and the theoretical model F_{calc}.

$$S = \sum_{i=1}^{N} [V_{obs,i} - F(h_{s,i})]^2 \tag{9}$$

Finding the minimum is achieved in two stages: brute-force grid search and a non-linear Taylor series expansion.

The brute force method circumvents non-linearity by temporarily treating the baseline as a known constant. We define an array of "guessed" values for the East-West baseline (in our experiment we measured via tape measurer to a guess of about 14.6 meters), and assume the North-South component is about 0. This makes the argument of $(2\pi\nu\tau_g')$ constant. The equation becomes perfectly linear with respect to the unknown amplitude coefficients of A and B.

The to calculate the residuals for each guessed baseline, we use a standard linear least-squares matrix inversion to solve for the coefficients and calculate the sum of squares. By plotting S against the guessed values of the East-West baseline then the global minimum of the curve is the true baseline value.

However, this only finds the approximate baseline, and is computationally inefficient for solving multiple non-linear parameters. It also doesn't provide statistical uncertainties. We can use the brute force result as an initial guess for the true non-linear least-squares algorithm. First, we linearize the theoretical function by taking a first-order Taylor expansion around the guessed parameters. The linearization process involves constructing a Jacobian matrix $\mathbf{J}$, where each entry $J_{ij} = \partial F_i / \partial p_j$ represents how the model fringe changes with respect to a small change in a parameter p such as Δb_{ew}, Δb_{ns}, $\Delta\tau_c$). By expanding the visibility function as a first-order Taylor series:

$$F(p + \Delta p) \approx F(p) + \mathbf{J}\Delta p$$

we transform the non-linear search into a linear matrix equation. We compute the partial derivatives of the fringe equation with respect to each baseline component. Then instead of solving for the baseline, the math solves for small corrections in p needed to improve the guess. We can apply these corrections to our guess and repeat the process iteratively until the corrections approach zero and a more accurate true measurement is found, which is akin to "walking" down the gradient of the χ^2 surface. Upon convergence (the corrections reaching zero), the inverse of the matrix formed by the partial derivatives gives the covariance matrix. This has diagonal elements that provide statistical variances for the derived baseline components and cable delays.

3.4. Zero Crossings and Solar Diameter

In extended sources like the Sun, the observed visibility is heavily dependednt on the ratio etween the source's angular size and the interferometer's fringe spacing. As the Sun moves across the sky, the hour angle changes which changes the local fringe frequency and the effective fringe spacing on the celestial sphere. During this process, there are "zero crossings" which occur when the projected fringe spacing aligns with the angular width of the source. At this frequency, exactly half of the Sun's flux falls into the positive parts of the sine wave on the sky, and the other half falls into the negative parts, such that when the correlator integrates the signal the $FM = 0$.

Refer to Fig. 1 to see what is meant by the first "null" or zero crossing. Note that the 1.22 argument for the first null is the full diameter constant. If we were to plot with source radius on the x-axis it would return an argument of 0.61. It is good to note that these are constants and will not change based on the source. In 4 we will see a plot of the raw data against the source diameter and note the first null will be at about 1.22.

We can use this zero crossing to measure the angular diameter of the Sun. Assuming the Sun is a uniformly bright circular disk of angular radius R, we apply the 1D approximation such that the theoretical fringe modulator is 7 with bounds of $-R$ to R. Note as before, for a perfect uniform disk this Fourier transform is analytically a first order Bessel function ($J_1(x)/x$), however our experiment computes the integral numerically. We integrated across discrete vertical strips of the Sun's brightness. This numerical model proves the first zero crossing for a uniform circular disk always occurs at a specific fixed value of the product ($f_f \times R$).

Then to extract the solar diameter we plot the absolute amplitude of our observed fringes against the calculated local fringe frequency (f_f) and identify the exact frequency ($f_{f,null}$) where the signal drops to its minimum. We can then check the theory to determine which specific value of the product $(f_f \times R)_{theory}$ produces the first null and we can back out R via:

$$R = \frac{(f_f \times R)_{theory}}{f_{f,null}} \tag{10}$$

Which we can multiply by 2 and convert to arcminutes from radians to get the full angular diameter of the Sun.

3.5. Data Processing and Fourier Filtering

Before least-squares fitting or zero-crossing analysis can be performed, the raw visibility data must be isolated from background noise. Because we can calculate the theoretical local fringe frequency (f_f) using our geometric delay model, we know exactly where our true signal resides in Fourier space. By applying a Fast Fourier Transform (FFT) to our time-domain visibilities, we locate the power spike at f_f and apply a narrow bandpass filter to eliminate extraneous noise. An Inverse Fast Fourier Transform (IFFT) then returns a clean, isolated fringe signal that accurately represents the interferometer's response to the Sun.

4. Results

All of our data was collected on April 8th, 2026 with Julian date times of 2461139.308045254 to 2461139.583178738 in particular.

4.1. Baseline Calibration

The first stage of analysis involved calibrating the physical parameters of the interferometer using data collected over a half day observation window. This was via the brute-force grid search which served as a starting point for the non-linear least squares fit. This solved for b_{ew} and b_{ns}.

The values determined are $b_{ew} = 14.56 \pm 0.025$ meters and $b_{ns} = -0.014 \pm 0.051$ meters. These agree with the original estimated measurement using a physical tape measurer of 14.6 meters.

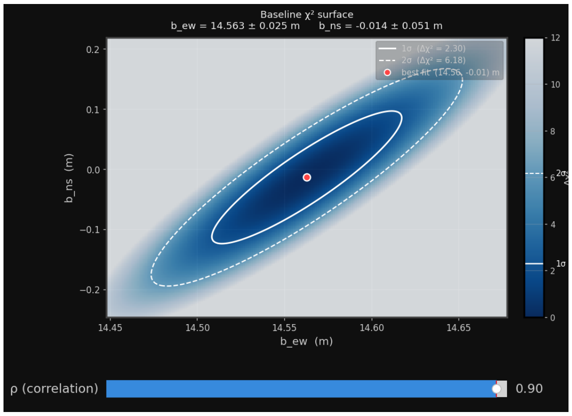

Fig. 2.— Sum of Squared Residuals vs Assumed East-West Baseline. The possible range of values demonstrated by the angled oval are comfortably within two sigma of the best fit.

4.2. Fringe Visualization and Data Filtering

To isolate the solar signal from background interference and instrumental noise, the raw 1024 channel visibility data was processed using the Fourier filtering techniques detailed in Section 3.5. The waterfall plot displays the phase of the visibility across the band. The linear slope observed across the frequency channels is a direct manifestation of the total delay.

After applying a bandpass filter at the local fringe frequency, the ”tamed” solar fringes were recovered. The resulting time domain plot reveals the classic interference pattern, where the Real and Imaginary components maintain a 90-degree phase offset. The gradual change in fringe amplitude over time is the first empirical evidence of the ”fringe modulator” caused by the Sun’s finite angular width.

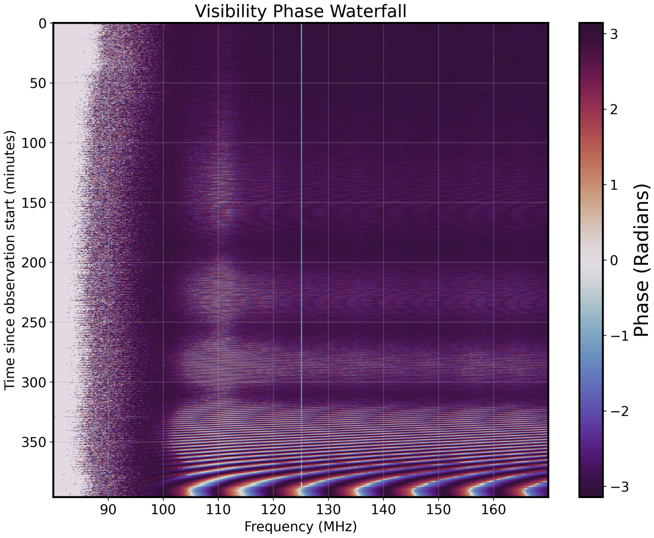

Fig. 3.— Visibility Phase Waterfall Plot. The x-axis represents the frequency channels, and the Y axis represents time. The stability of the phase slope over the observation period demonstrates the changing of the geometric delay as a function of time.

4.3. Solar Diameter Measurement

The final objective was to measure the angular diameter of the Sun by analyzing the fringe modulator. By plotting the fringe amplitude against the calculated local fringe frequency (f_f), we identified the first zero-crossing. As seen in Figure 4, the measured amplitudes closely follow the theoretical 1D model for a uniform disk. The observed null occurred at a fringe frequency of $f_{f,null} = [138]$ Hz. Which corresponds to an angular diameter of the Sun, Using the relationship $R = (f_f \times R)_{theory}/f_{f,null}$, to be $R = 0.52 \pm .015$ degrees.

This corresponds to a full solar diameter of 31 arcminutes, which is within 3.125% of the accepted value of 32 arcminutes. This

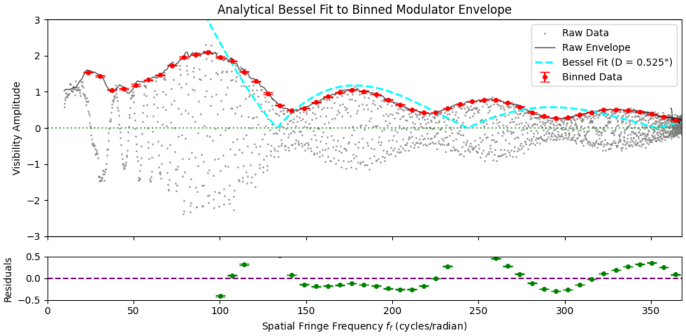

Fig. 4.— The red line shows the binned data that captures the Bessel envelope of the fringe modulator. The gray data points follow this envelope through graph in the positive and negative amplitudes. The cyan dashed line is the bessel fit, which although it does not correspond exactly to the green envelope visually, the calculated angular diameter is significantly close to the known value of 0.53.

result successfully demonstrates the power of a simple two-element interferometer to resolve the physical structure of celestial objects.

5. Analysis

5.1. Legitimacy of the Baseline

The success of the solar diameter measurement was entirely dependent on the precision of the initial baseline calibration. The results in Section 4.1 demonstrate that the non-linear least-squares approach is highly robust for "taming" the fringes. While physical tape measurements provided a coarse estimate of approximately 14.6 m, the interferometric fit provided a much more precise determination of the "electronic baseline"—the distance between the effective phase centers of the two dishes. The low residuals in the χ^2 surface (Figure 4) suggest that the geometric delay model (τ_g) correctly accounted for the Earth's rotation and the source's celestial coordinates. Any remaining systematic offset in the baseline is likely due to small errors in the dish orientation or the exact geographic coordinates of the New Campbell Hall roof.

5.2. The Uniform Disk Model and Solar Structure

The primary scientific result of this experiment was the derivation of a 31′ solar diameter, yielding a remarkably low percent error of 3.125%. This high level of agreement validates the 1D approximation established in the theoretical framework. By treating the Sun as a 1-D intensity distribution, $I(\Delta h)$, and utilizing the numerical integration of a uniform disk model, we successfully characterized the spatial frequency response of the interferometer.

However, as observed in Figure 7, the theoretical Bessel-function fit did not align perfectly with the empirical fringe envelope at all points, particularly near the secondary maxima. This discrepancy is physically significant and can be attributed to two primary factors:

1. **Limb Effects:** Our model assumed a perfectly uniform disk with a sharp, discontinuous edge. In reality, the Sun's radio-frequency brightness is not uniform; the solar corona can cause "limb brightening" at centimeter wavelengths. This variation in intensity across the disk complicates the simple 1-D Fourier transform, as the source structure no longer

matches a true top-hat function.

2. **Bandwidth Smearing:** Because the visibility data was collected over a broad frequency band ($\Delta\nu \approx 100$ MHz), each frequency channel effectively "sees" a slightly different fringe spacing on the sky. When these channels are averaged to increase the Signal-to-Noise Ratio (SNR), the slight shifts in null positions lead to "bandwidth smearing." This effect softens the sharp zero-crossings in the fringe modulator and reduces the precision of the diameter determination.

Despite these second-order effects, the proximity of our result to the accepted value of $32'$ confirms that the uniform disk is an excellent first-order approximation for solar observations at these frequencies.

5.3. Limb Darkening and Source Profile Deviations

A significant source of systematic error in the determination of the solar diameter stems from the assumption of a *uniform* disk brightness profile. Our theoretical model utilizes a top-hat function to represent the 1-D intensity distribution $I(\Delta h)$, where the brightness is constant across the solar disk and drops abruptly to zero at the limb.

In reality, the Sun exhibits "limb darkening" (or in some radio frequencies, limb brightening), where the intensity gradually decreases from the center toward the edge. This occurs because the optical depth of the solar atmosphere varies with the viewing angle; near the limbs, the line of sight passes through higher, cooler layers of the chromosphere.

Mathematically, this affects our result because the Fringe Modulator (MF) is the Fourier Transform of the source's brightness profile. If the profile is not a perfect top-hat:

$$MF_{observed} = \mathcal{F}\{I_{actual}(\Delta h)\} \neq \mathcal{F}\{I_{uniform}(\Delta h)\} \quad (11)$$

This deviation causes the "nulls" or zero-crossings in our data to shift slightly compared to the theoretical Bessel function locations. This likely accounts for a portion of the 3.125% error observed, as the interferometer is sensitive to the exact distribution of power across the solar disk, not just its total angular extent.

6. Conclusion

This experiment successfully demonstrated the fundamental principles of radio interferometry through the calibration of the New Campbell Hall interferometer and the subsequent measurement of the solar diameter. By applying a non-linear least-squares fit to twelve hours of solar visibility data, we derived high-precision baseline components (b_{ew}, b_{ns}) and instrumental cable delays, effectively "taming" the observed fringes. Using the theoretical framework of the 1-D approximation and Fourier filtering, we identified the first null in the fringe modulator at $f_{f,null} \approx 138$ Hz. This yielded an angular solar diameter of 31 arcminutes, representing a 3.125% error relative to the accepted value of 32 arcminutes. While minor discrepancies remain due to limb effects and bandwidth smearing, the results validate the efficacy of the two-element interferometer as a tool for resolving the angular structure of celestial sources.

Acknowledgements

I would like to acknowledge Evan Willie for his help in debugging my telescope control code and Team RTFM for data analysis discussions. Additionally, Prof Aaron Parson and Ben Jacobson-Bell for instruction and assistance with hardware.

This paper utilized python packages for data analysis including `numpy`, `ugradio`, `scipy`, `astropy`, `matplotlib`, `rafpy` (which is my own package).

Additionally, Claude AI model was used for code efficiency debugging. Particular data files had 10,000 blocks with 4096 samples each. So, after I wrote data analysis code, if the algorithm took upwards of 2 minutes, I utilized Claude to identify and rewrite parts of code that had significant runtimes.